RSC Advances

PAPER

View Article Online
View Journal | View Issue

Cite this: *RSC Adv.*, 2019, **9**, 25480

Porous carbon material derived from fungal hyphae and its application for the removal of dye†

Siji Chen,[ab] Zhixiao Wang,[ab] Yuhan Xia,[ab] Bolun Zhang,[ab] Huan Chen,[ab] Guang Chen*[ab] and Shanshan Tang *[ab]

Received 21st June 2019
Accepted 3rd August 2019

DOI: 10.1039/c9ra04648h

rsc.li/rsc-advances

In this work, fungal hyphae (FH, *Irpex lacteus*) was used as the carbon resource for the preparation of porous carbon materials (PCFH) using mixed alkali as the activator. The SEM, N_2 adsorption/desorption, FT-IR, XRD, Raman, and XPS were used to characterize the structure and surface properties of PCFH. The results showed that the PCFH not only has a huge Brunauer–Emmett–Teller (BET) surface area (2480 m^2 g^{-1}), but also has abundant functional groups containing carbon, oxygen, and nitrogen. Rhodamine B (RhB) was selected to evaluate the adsorption properties of the PCFH prepared under different conditions in dyeing wastewater. A fast adsorption rate was observed, and an uptake capacity of 765 mg g^{-1} was achieved in the initial 5 min. The maximum adsorption capacity of PCFH to RhB reached 1912 mg g^{-1} at the pH value of 9, which could efficiently remove RhB from the aqueous solution. The adsorption process was fitted better by a pseudo-second order model, and the adsorption isotherm for the RhB was well fitted by the Freundlich model. Moreover, the probable mechanism of adsorption was analyzed. In short, the good adsorption performance of PCFH indicated that it has a broad application prospect for dye water pollution control.

1. Introduction

Biomass carbon is a carbon-rich product which is derived from biomass *via* high temperature pyrolysis (without oxygen or with limited oxygen content).[1] Recently, it has become a research hotspot[2–6] due to its unique advantages (huge specific surface area and abundant functional groups, *etc.*) and wide applications[7,8] (catalysts, adsorbents, separation materials, gas and energy storage materials, electrochemical materials, *etc.*). Over the past few decades, materials scientists have been working hard to produce fascinating materials and structures inspired by nature,[9–11] and have made countless gains in the field of abundant biomass carbon materials.[12] To date, there are still great concerns with the development of new carbon sources and the preparation of biomass carbon materials with better performances.

Up to now, a large amount of works can be found about using biomasses as carbon sources to prepare porous carbon (PC) including rapeseed dregs,[13] bamboo leaves,[14] orange peel,[15] clover stems,[16] quinoa husk,[17] corn straw,[18] and the like. However, there is still little research has been done on carbon based on microorganisms, such as bacteria, fungi, viruses, *etc.*[12] Among the microorganisms, fungal hyphae (FH) has attracted special attention because of unique advantages. On the one hand, it is because of its strong sustainable production capacity. On the other hand, it is formed by the germination of fungal spores. Then it eventually forms a three-dimensional network structure.[19] In recent studies, the carbon nanotubes (CNTs) was loaded onto FH to prepare sphere FH/CNTs composite and the maximum adsorption amounts of FH/CNTs composites for uranium, congo red, and methyl violet reached 187.26, 43.99 and 20.89 mg g^{-1}, respectively.[20] The graphene oxide, Fe_3O_4 particles, and FH were fixed to prepare a composite and the maximum adsorption capacity of methyl violet and uranium were calculated to be 117.35 and 219.71 mg g^{-1}.[21] After anchor TiO_2 and Fe_3O_4 particles onto the FH, the adsorption capacity of the composite to tannin reached 45.61 mg g^{-1}.[22] However, in above work, FH was only used as a carrier for producing composite materials, and the potential of FH for preparing porous carbon materials has not been explored.

Environmental pollution, especially industrial wastewater pollution, has become a global environmental problem. In general, industrial wastewater contains various pollutants, especially synthetic dyes, which are believed to not only interfere with sunlight entering water and hinder photosynthesis, but also affect the solubility of gas in water and inhibit the growth of aquatic organisms.[23,24] Adsorption has always been one of the most commonly used strategies for removal of dyes

[a]*College of Life Sciences, Jilin Agricultural University, Changchun 130118, China. E-mail: 18638342679@163.com; wzx19950628@163.com; 18543718988@163.com; aa921526347@163.com; chjlau@163.com; chg61@163.com; tangshanshan81@163.com*

[b]*The Key Laboratory of Straw Biology and Utilization, The Ministry of Education, Jilin Agricultural University, Changchun 130118, China*

† Electronic supplementary information (ESI) available. See DOI: 10.1039/c9ra04648h

due to its simple principle and convenient use. Although many adsorbents derived from biomass carbon have been developed to remove dyes,[25,26] it is still a challenge to obtain carbon materials with larger surface area and better adsorption performance through simpler and more environmentally friendly methods.

In this work, FH was used as the raw material for preparing PC. After FH was carbonized, the mixed alkali consisted of KOH and NaOH was used as the activator to prepare porous carbon based on FH (PCFH). The activation conditions of PCFH preparation were explored and optimized. The physical and chemical properties of the prepared PCFH were characterized. In addition, the batch adsorption experiments of Rhodamine B (RhB) were carried out to study the adsorption performance and mechanism under different conditions, and the effectiveness of the material was verified. Furthermore, the adsorption capacity of PCFH to RhB is higher than the other adsorbents in the present study, which proved that the PCFH has potential application values in the pollution control of industrial dye wastewater.

2. Experimental

2.1 Materials

Irpex lacteus was obtained from a decayed corn straw pile by Technological innovation platform of straw comprehensive utilization in Jilin province. The potato was obtained from the local supermarket. The D-glucose monohydrate was provided by Sinopharm Group Chemical Reagent Co., Ltd. (Shanghai, China).

All reagents used in the experiment were of analytical purity and used without further purification. KOH, NaOH, and HCl were provided by Beijing Chemical Works (Beijing, China). RhB was provided by Aladdin Chemical (Shanghai) Co., Ltd. (Shanghai, China). Deionized water was used in all preparation and flushing processes.

2.2 Preparation of PCFH

The fungus was cultured on a Potato-Dextrose-Agar (PDA) solid medium (200 g L^{-1} of potato extract, 20 g L^{-1} of D-glucose, and 20 g L^{-1} of agar) for 5 days at 28 °C. Then the grown fungus was inoculated from the agar-plate into a 15 mL liquid PDA medium (200 g L^{-1} of potato extract and 20 g L^{-1} of D-glucose) plate for growth to form a large number of FH. Incubation was carried out in the 28 °C constant temperature incubator for 7 days. After separated from the medium, the FH were washed with deionized water for removal of dusts and water-soluble impurities, and then it was dried at 80 °C for 24 h. These FH were used for the subsequent experiments.

The dried FH were calcined under the N_2 atmosphere at 600 °C with a heating rate of 10 °C min^{-1} for 60 min (according to the result of thermal gravimetric analyses Fig. S1†). When the carbonization furnace was cooled to the room temperature, the carbonized FH (CFH) were taken out. Then the CFH was mixed with the alkali at the different ratios (the PCFH, PCFH-3:0:1 and PCFH-0:3:1 mean that the composite ratios of KOH : NaOH : carbon are 1.5 : 1.5 : 1, 3 : 0 : 1, and 0 : 3 : 1, respectively). The mixture samples were heated to the activation temperature of 700 °C under N_2 flow (the PCFH, PCFH-600, and PCFH-800 mean that the activation temperatures are 700, 600, and 800 °C, respectively), and held at the corresponding temperature for 60 min (the PCFH, PCFH-30, and PCFH-90 mean that the activation times are 60, 30, and 90 min, respectively). The PCFH was washed with 0.1 mol L^{-1} HCl solutions and deionized water until a neutral pH value of about 7 was reached. Then, the PCFH was dried at 180 °C for 12 h and kept in a desiccator prior to adsorption.

2.3 Adsorption experiments

2.3.1 Adsorption kinetics. The adsorption capacities of FH and PCFH prepared under the different conditions were investigated to select the model sample to study the adsorption performance. In a typical experiment, 10 mg samples were added to a flask containing 100 mL dye solution of different initial concentrations (40, 80, 120, 160, and 200 mg L^{-1}). The flasks were performed in an air-heated shaking table in dark with 150 rpm at the ambient temperatures of 303 K, and the time intervals used were from 0 to 150 min. At each adsorption time, 2 mL samples were subjected to centrifugation at 12 000 rpm for 5 min and the suspensions were filtered, diluted. The concentrations of dye solutions were calculated by measurement the absorbance of RhB at wavelength of 554 nm *via* the UV-Vis spectrophotometer (Agilent Cary300, USA). All adsorption experiments were performed in duplicate. The equilibrium adsorption capacity Q_e (mg g^{-1}) was calculated with the following eqn (1):[27]

$$Q_e = \frac{(C_0 - C_e) \times V}{W} \quad (1)$$

C_e (mg L^{-1}) and C_0 (mg L^{-1}) mean the equilibrium and the initial concentrations of the dye, respectively. V (L) and W (g) are the volume of the dye solution and the weight of the adsorbent, respectively.

2.3.2 Adsorption isotherms. To evaluate the effects of initial dye concentration on the adsorption, 10 mg samples were added to a flask containing 100 mL dye solution of different initial concentrations (40, 80, 120, 160, and 200 mg L^{-1}). The flasks were agitated in an air-heated shaking table in dark with 150 rpm for 120 min at different temperatures (298, 303, and 313 K). The concentrations of dye solutions were calculated by measurement the absorbance of RhB at wavelength of 554 nm *via* the UV-Vis spectrophotometer (Agilent Cary300, USA).

2.3.3 Effects of pH. The effect of pH on the adsorption was evaluated. Different pH values (3, 5, 7, 9, and 11) were obtained by adjusting the dye solution (400 mg L^{-1}) with HCl or NaOH solution. The flasks were agitated in an air-heated shaking table in dark with 150 rpm for 120 min at 303 K. After filtration and diluted, the concentrations of dye solutions were calculated by measurement the absorbance of RhB at wavelength of 554 nm *via* the UV-Vis spectrophotometer (Agilent Cary300, USA).

2.4 Characterization methods

Thermal gravimetric analyses (TGA) was carried out using a thermal gravimetric analysis instrument (TA SDTQ600 from USA) under the N_2 flow at a heating rate of 10 °C min^{-1}. The morphology of samples were performed by a scanning electron microscopy (SEM) (JSM-6700F from Japan). The N_2 adsorption/desorption isotherms were carried out at 77 K by using a surface area and pore size analyzers (Micromeritics ASAP 2460 Version 2.02 from USA). The specific surface area was calculated on the basis of the Brunauer–Emmett–Teller (BET) method and the pore size was calculated from the adsorption branch of the isotherm based on the Barrett–Joyner–Halenda (BJH) model. Fourier transform infrared (FT-IR) patterns were obtained at a resolution of 1 cm^{-1} between 400 and 4000 cm^{-1} by using a spectrometer (Thermo Nicolet NEXUS 410 from USA). Powder X-ray diffraction (XRD) pattern was measured using a diffractometer with Cu-Kα X-ray source (Bruker D8 advance from Germany). Raman study of the carbon material was carried out with the laser wavelength of 514 nm using an inVia Reflex Raman spectrometer (Renishaw from UK). The X-ray photoelectron spectra (XPS) were carried out on an electron energy spectrometer (Thermo Escalab 250Xi from USA). The suspension after adjusting pH from 3 to 11 by adding HCl and NaOH was determined by using a zeta potential Zetasizer Nano ZS90 from Malvern Instruments in UK.

3. Results and discussion

3.1 Characterization

Filamentous fungi is a kind of renewable resources with fast growth, low cost, easy access and environmental friendliness. Recently, it was reported that FH can grow into uniform long fiber with the characteristics of microscale and large scale.[19,20] Fig. 1 shows the morphology and microstructure of the FH, CFH, and PCFH. As can be seen from Fig. 1a, *Irpex lacteus* has a white surface with a large number of slender hyphae fibers. These filaments form the basis of the three-dimensional carbon network.[19] From the microscopic perspective (Fig. 1b and c), FH and CFH are composed of columnar microfibers with sizes of about 3 μm and 1 μm, respectively. The difference in carbon fiber size can be explained that the successful dehydration and carbonization of FH after pyrolysis at 600 °C. Fig. 1d shows that the PCFH still maintains the carbon network structure after the activation. In addition, a large number carbon network structures of PCFH have fracture and appear pores.

N_2 adsorption–desorption has been used to investigate the porous structure of CFH and PCFH prepared at different conditions (Fig. 2a, Table 1, and Fig. S2†). PCFH prepared at different conditions show typical type-IV isotherm (Fig. 2a),[28] which means that not only there are a lot of the mesopores, but also an amount of micropores exist in PCFH with different preparing conditions (0.29, 0.34, 0.42, 0.56, 0.34, 0.54, and 0.41 cm^3 g^{-1}). The BJH method is used to investigate the mesopore distribution, and the volume of mesopores is very high, which could above 2 nm to 50 nm (Fig. S2†). The pore sizes of PCFH prepared at the different conditions focus on 2.58, 2.61, 2.83, 3.15, 2.70, 2.77, and 2.82 nm, respectively, indicating that the mesoporous structure occupies the major part in the PCFH (Table 1). Interestingly, the average pore sizes of PCFH are slightly larger than that of RhB (1.8 nm). These pores may be able to provide pore filling sites for the adsorption representative dye RhB. The specific surface area of CFH is 3.32 m^2 g^{-1}. This implies that the large specific surface area does not come from carbonization, which is in agreement with the results of literatures.[18,29–31] While on the contrary, PCFH show the large specific surface areas of 2480, 1628, 1594, 1763, 1797, 1540, and 1945 m^2 g^{-1}, respectively, which demonstrates

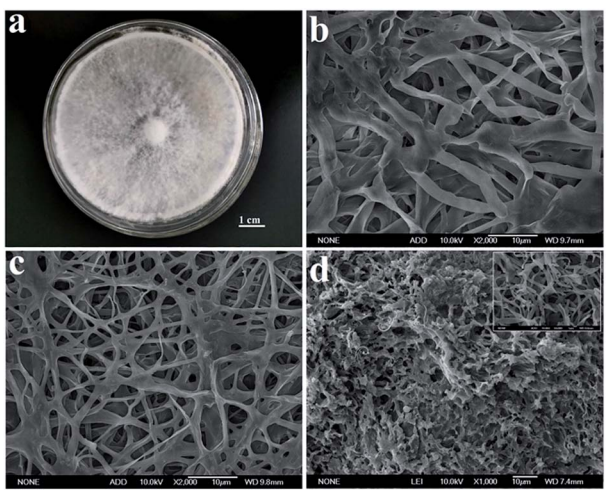

Fig. 1 Digital photo of (a) FH grow in a medium plate, SEM images of (b) FH, (c) CFH, and (d) PCFH.

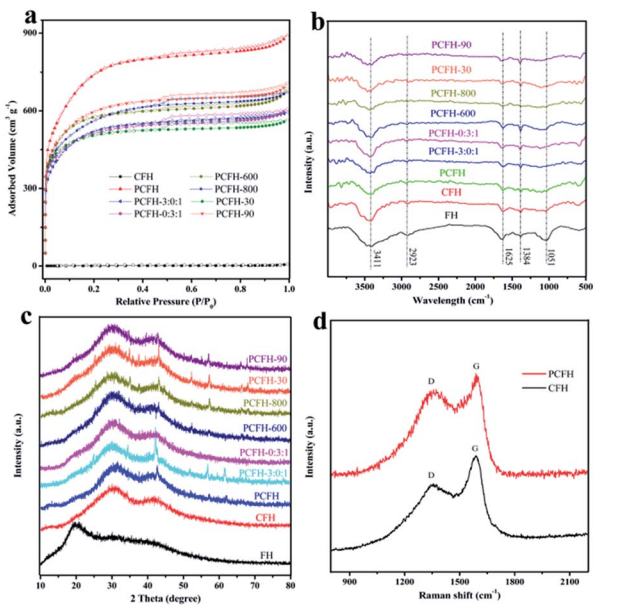

Fig. 2 (a) N_2 adsorption–desorption isotherms, (b) FT-IR spectra, and (c) XRD pattern of FH, CFH, and PCFH prepared at different conditions. (d) Raman spectra of CFH and PCFH.

Table 1 The data of N_2 adsorption for CFH, PCFH prepared at different conditions[a]

	Conditions						
Samples	KOH : NaOH : carbon	T (°C)	t (min)	S_{BET} (m^2 g^{-1})	Pore size (nm)	V_{micro} (cm^3 g^{-1})	V_{total} (cm^3 g^{-1})
CFH	—	600	60	3.32	15.02	0.0012	0.0052
PCFH	1.5 : 1.5 : 1	700	60	2480	2.58	0.29	1.33
PCFH-3:0:1	3 : 0 : 1	700	60	1628	2.61	0.34	0.90
PCFH-0:3:1	0 : 3 : 1	700	60	1594	2.83	0.42	0.90
PCFH-600	1.5 : 1.5 : 1	600	60	1763	3.15	0.56	1.00
PCFH-800	1.5 : 1.5 : 1	800	60	1797	2.70	0.34	1.01
PCFH-30	1.5 : 1.5 : 1	700	30	1540	2.77	0.54	0.85
PCFH-90	1.5 : 1.5 : 1	700	90	1945	2.82	0.41	1.04

[a] S_{BET} (m^2 g^{-1}) is the BET surface area, V_{micro} (cm^3 g^{-1}) is the volume of micropore, and V_{total} (cm^3 g^{-1}) is the total pore volume.

that the successfully activation could give huge specific surface area for PCFH. As we can see from the Fig. 2a and Table 1, the PCFH, activated at 700 °C for 60 min *via* mixed alkali, has the best performance among these PCFH prepared at the different conditions (activation temperature, activation time, and the ratio of mixed alkali). The specific surface area and total pore volume of PCFH could reach 2480 m^2 g^{-1} and 1.33 cm^3 g^{-1}, respectively, which could explain that the PCFH could be regarded as a porous carbon material.[29,30]

FTIR spectroscopy was always used to evaluate the surface chemistry of the carbon materials.[31,32] As can be seen from Fig. 2b, the FT-IR spectra of samples showed some peaks at 3411 (–OH stretching bond of hydroxyl groups),[20] 2923 (stretching vibrations of CH, CH_2, and CH_3 groups),[21] 1384 (the N–H bending from the amide group),[33] 1625 (C=O stretching band of carbonyl groups),[34] and 1051 (C–O–C component)[35] cm^{-1}, which were attributed to the physically adsorbed water molecules, the lipids,[33] the amide of proteins and chitin,[34] and the polysaccharides,[35] respectively. These results show that there are no obvious differences among the PCFH samples prepared under different conditions. It reveals that the basic structures of PCFH do not change in the carbonization and activation processes.

From XRD pattern (Fig. 2c) and Raman spectra (Fig. 2d), one can find that the CFH and PCFH are amorphous structures, which likes most of biomass derived carbon materials.[30,36–38] As shown in Fig. 2c, the characteristic peaks of PCFH appearing at 30.1 and 43.5° are attributed to the planes of hexagonal graphitic carbon,[19] implies its amorphous nature with the absence of peaks. Moreover, the XRD patterns of samples did not change significantly under different conditions. The Raman spectra of CFH and PCFH (Fig. 2d) show two remarkable peaks at 1322 cm^{-1} (D) and 1588 cm^{-1} (G), corresponding to the amorphous carbon with smaller size and the crystalline graphite structure of carbon material, respectively.[21] The intensity ratio of the D band (I_D) to G band (I_G) is usually calculated to evaluate the extent of defects and disorder in carbon materials.[39] The huge D peak indicates that there are numerous amorphous carbon exist in CFH and PCFH. Even more interesting, the value of I_D/I_G changed from 1.24 to 1.68, which reveals that more amorphous carbon was formed in PCFH than in CFH.

As can be seen from Fig. 3a, PCFH is similar to many biomass carbon materials,[7,12] and also contains C, O, N, P and other elements. FH with different treatment methods has different contents of elements (Table S1†). Table S1† shows that the contents of C, O, N, and P are 91.51%, 6.75%, 1.69%, and 0.05%, respectively. Fig. 3b, c, and d show the C1s, the O1s, and the N1s of the PCFH, respectively. The high-resolution C1s spectra of PCFH (Fig. 3b) can be fitted into three carbon functional groups, which are C–C (284.8 eV), C–OH (286.0 eV), and C=O (287.8), respectively. The high-resolution O1s spectra of PCFH could be divided into two different carbon–oxygen groups, which are O=C (532.8 eV) and O=C–O (531.8 eV). Obviously, Fig. 3d shows two kinds of nitrogen atoms in PCFH, namely pyrrolic N (399.7 eV)[16] and graphitic N (400.9 eV),[15] which may be derived from the amide of proteins and chitin.[19] The results of XPS are basically consistent with those of FT-IR.

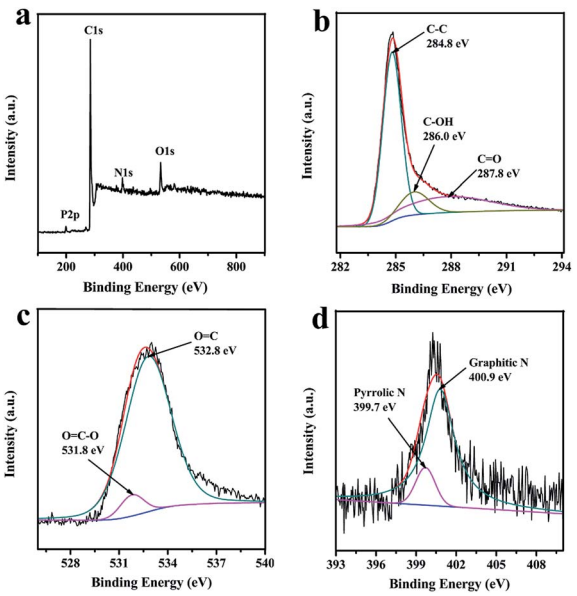

Fig. 3 (a) XPS spectra, (b) the C1s, (c) the O1s, and (d) the N1s of the PCFH.

3.2 Adsorption properties

3.2.1 Adsorption kinetics. The adsorption capacities of FH and PCFH prepared under the different conditions (Fig. S3;† dye: RhB; C_0: 400 mg L^{-1}; V: 100 mL; pH: 3.4 ± 0.1; adsorbent: 10 mg) have been investigated. Biomass carbon does not always perform better than biomass adsorbents. For some pollutants such as heavy metals,[9–11] the adsorption capacity of biomass carbon is not very high. In addition, the treatment of biomass adsorbents is more energy efficient than the preparation of biomass carbon (microwave pyrolysis, hydrothermal synthesis, and high-temperature pyrolysis).[2–6] But in terms of this material (fungal hyphae, *Irpex lacteus*), PCFH is better than FH (Table S2†). After carbonization–activation treatment, PCFH has a large specific surface area and higher porosity than FH, which can improve the adsorption capacity to RhB by providing more adsorption sites. Thus, the PCFH (activation conditions: KOH : NaOH : carbon = 1.5 : 1.5 : 1, 700 °C, 60 min) with the highest adsorption capacity (1509 mg g^{-1}) was selected as the object model to study the adsorption performance. The results of adsorption kinetics and the kinetics models of PCFH to RhB at 303 K are shown in Fig. 4. As we can see from Fig. 4a, the adsorption trend of RhB with different concentrations are the same and the adsorption capacity remarkably increase with the initial concentration increasing. The adsorption capacity increased sharply in the first 20 min and gradually achieved equilibrium in 120 min, indicating that the adsorption of PCFH to RhB was a rapid adsorption.

In order to study the adsorption rate, an important parameter of adsorption performance, three kinetics models including the pseudo-first-order kinetic, the pseudo-second-order kinetic, and intra-particle diffusion model have been investigated (Fig. 4b–d) and the data were fitted (Table 2).

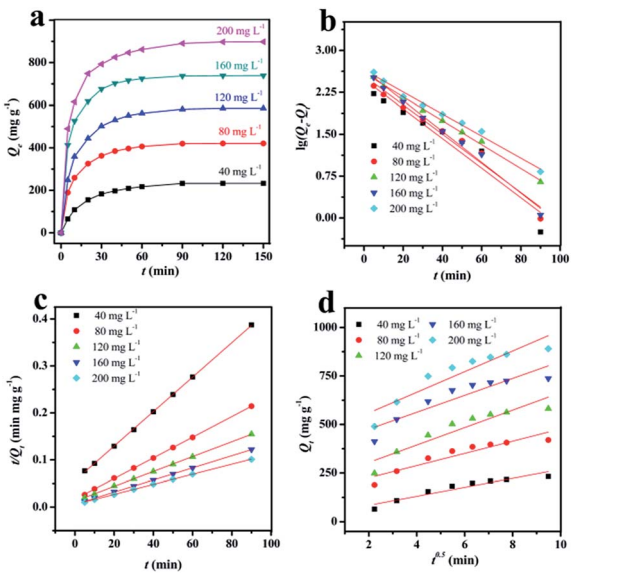

Fig. 4 (a) The adsorption kinetics of PCFH to RhB at 303 K. (b) Pseudo-first-order kinetic plots, (c) pseudo-second-order kinetic plots, and (d) plots of intra-particle diffusion model.

Lagergren's pseudo-first-order can be expressed as the following eqn (2):

$$\lg(Q_e - Q_t) = \lg Q_e - \frac{K_1}{2.303} t \quad (2)$$

K_1 (g mg^{-1} min^{-1}) is the first-order rate constant. Q_e and Q_t (mg g^{-1}) are the equilibrium adsorption capacities and the adsorption capacities at time t (min), respectively. The values of the correlation coefficient R^2 obtained were between 0.96–0.99 and the Q_e were higher than the calculated $Q_{e.cat}$. These results show that the Lagergren's pseudo-first-order might be not suitable for the adsorption of PCFH to RhB.

The pseudo second-order model is expressed by eqn (3):

$$\frac{t}{Q_t} = \frac{1}{K_2 Q_e^2} + \frac{t}{Q_e} \quad (3)$$

K_2 (g mg^{-1} min^{-1}) is the second-order rate constant. Q_e can be calculated from the slope of the plot obtained by plotting t/Q_t *versus* t. The Fig. 4c shows a good linear relationship between t/Q_t and t with the R^2 range of 0.99–0.99 (Table 2) and the calculated $Q_{e.cat}$ were basically consistent with the Q_e, which implied the adsorption of PCFH to RhB may follow the pseudo second-order model. This situation also suggests that the adsorption of PCFH to RhB may exist a chemical adsorption, which through the sharing or exchange of electrons between the dye and the adsorbent.[40]

Intra-particle diffusion model can be expressed as eqn (4):

$$Q_t = K_3 t^{0.5} + C \quad (4)$$

K_3 (mg g^{-1} $min^{-0.5}$) is the intra-particle diffusion rate constant. C (mg g^{-1}) is a constant which could reveal the thickness of the boundary layer. The Fig. 4d and Table 2 show the poorest linear relationship between Q_t and $t^{0.5}$ with the R^2 range from 0.84 to 0.92. The results suggest that the adsorption of PCFH to RhB may not follow the intra-particle diffusion model.

3.2.2 Adsorption isotherms. The two adsorption isotherm models, Langmuir isotherm model and Freundlich isotherm model, have been applied to study the properties of PCFH (Fig. 5 and Table 3). They were expressed in eqn (5) and (6) respectively.

Langmuir isotherm model, which presumes that the adsorption would occur only at the specific-site on the surface and the adsorbate would monolayer coverage the surface of adsorbent.[41] The model can be expressed as eqn (5):

$$Q_e = \frac{Q_m K_L C_e}{1 + K_L C_e} \quad (5)$$

Q_e is the equilibrium adsorption capacity of PCFH (mg g^{-1}). Q_m is the maximum adsorption capacity (mg g^{-1}). C_e is the equilibrium concentration of dye in solution (mg g^{-1}). K_L is related to adsorption energy Langmuir constant (L g^{-1}). The values of the correlation coefficient R^2 were 0.95, 0.96 and 0.88 for 293, 303, and 313 K, respectively. The poor linear relationship suggests that the adsorption of PCFH to RhB may not follow the Langmuir isotherm model.

Unlike the Langmuir isotherm model, Freundlich isotherm model assumes the adsorption is not limited to the monolayer.

Table 2 Fitting parameters of the pseudo-first-order equation, the pseudo second-order model, and intra-particle diffusion model

		Pseudo-first-order kinetic			Pseudo-second-order kinetic			Intra-particle kinetic		
C_0 (mg L^{-1})	Q_e (mg g^{-1})	K_1 (min^{-1})	$Q_{e.cat}$ (mg g^{-1})	R^2	K_2 (g mg^{-1} min^{-1})	$Q_{e.cat}$ (mg g^{-1})	R^2	K_3(mg g^{-1} $min^{-0.5}$)	C	R^2
40	252.65	0.0610	173.54	0.97	0.0002	270.27	0.99	23.01	38.69	0.92
80	426.66	0.0603	216.92	0.97	0.0003	454.55	0.99	30.93	162.51	0.87
120	594.98	0.0493	330.37	0.98	0.0002	625.00	0.99	44.98	214.02	0.87
160	748.24	0.0636	371.71	0.96	0.0003	769.23	0.99	43.64	388.28	0.84
200	895.18	0.0454	477.97	0.99	0.0002	909.09	0.99	53.24	452.91	0.86

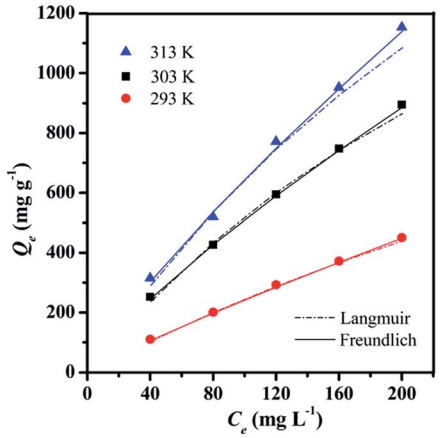

Fig. 5 Adsorption isotherms of PCFH to RhB at 293, 303, and 313 K, respectively.

Table 3 Fitting parameters of the Langmuir and Freundlich isotherm models

		Temperatures (K)		
Isotherm models	Constants	293	303	313
Langmuir	Q_m (mg g^{-1})	2000	2500	3333
	K_L (L mg^{-1})	0.0014	0.0027	0.0024
	R^2	0.95	0.96	0.88
Freundlich	K_F (mg g^{-1} (L mg^{-1})$^{1/n}$)	4.3231	13.7088	15.3356
	n	1.1388	1.2694	1.2285
	R^2	0.99	0.99	0.99

It is widely used to describe heterogeneous surface adsorption due to the presence of different functional groups on the surface.[42] The model is given as eqn (6):

$$Q_e = K_F C_e^{1/n} \quad (6)$$

K_F and $1/n$ are Freundlich constants corresponding to adsorption capacity and heterogeneity factor, respectively. The linear relationship of Freundlich isotherm model is better than that of Langmuir isotherm model can be seen from Fig. 5. The correlation coefficient R^2 were 0.99, 0.99, and 0.99 for 293, 303, and 313 K, respectively (Table 3). Besides, the n values of PCFH at 293, 303, and 313 K were 1.1388, 1.2694, and 1.2285, respectively. It indicates when the n value is larger than 1, the adsorption conditions are proper. Moreover, the adsorption of PCFH to RhB was heterogeneous surface adsorption, which is caused by the different functional groups on the surface of PCFH. Thus, the adsorption of PCFH to RhB may obey Freundlich isotherm model.

3.2.3 Effect of pH and comparison with other adsorbents. The pH value of solution is an important parameter, which affects significantly the adsorption capacity of adsorbent to dye.[43,44] Fig. 6a shows the variation in the adsorption capacity of PCFH to RhB and the zeta potential of PCFH with the initial solution pH ranging from 3 to 11. The adsorption capacity of PCFH to RhB decreases significantly along with the solution pH value increasing from 3 (1613 mg g^{-1}) to 5 (1390 mg g^{-1}) and from 9 (1912 mg g^{-1}) to 11 (1670 mg g^{-1}). However, the adsorption capacity of PCFH to RhB increases significantly when the pH value increases from 5 to 9. The changes of solution pH values would affect not only the surface charge of PCFH, but also the molecular charge of RhB in aqueous solution.[45] With increase of the pH values from 3 to 5, the surface charge of PCFH became negative. At the same time, the formation of molecular dimers of RhB was accelerated by zwitterionic form of RhB in the solution with pH value of 3–5, owing to electrostatic attractions between $-COO^-$ and $-N^+$ of monomers.[46] As a result, it is more difficult for larger molecules to enter the pores of PCFH, resulting in the decrease of the adsorption capacity of PCFH to RhB. As the pH value further increased from 5 to 9, the preponderance of OH^- in the solution would compete with $-COO^-$ to combine with $-N^+$, it will hinder the aggregation of RhB, which will improve the adsorption capacity of PCFH to RhB.[47] When the pH values are higher than 9, the capacity of PCFH to RhB significantly decreased due to the electrostatic repulsion between RhB and PCFH with negative charges. Based

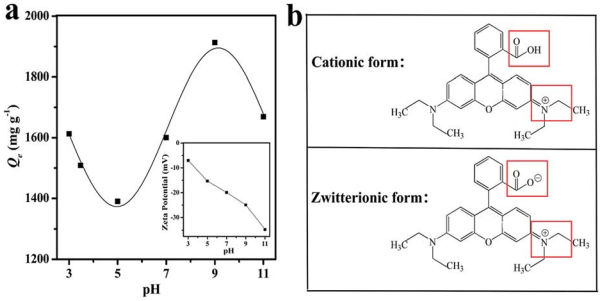

Fig. 6 (a) The effect of pH on the adsorption of RhB and the zeta potential of PCFH (inset). (b) Different molecular forms of RhB.

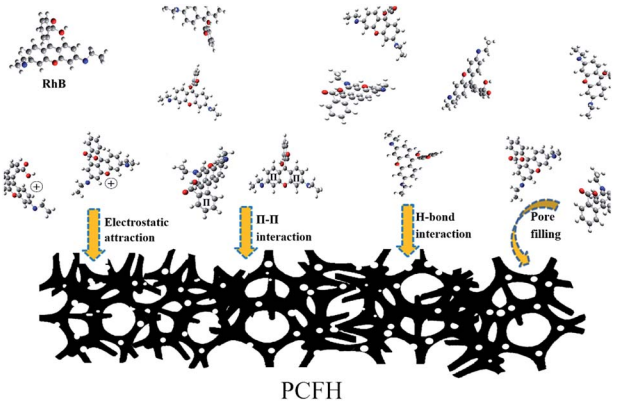

Fig. 7 The adsorption mechanism diagram of PCFH to RhB.

on these results, the adsorption capacity of PCFH to RhB at the pH value of 9 was determined to be the best.

3.3 Probable mechanism analysis

The schematic diagram of the major adsorption mechanism of PCFH to RhB is shown in Fig. 7. In this work, the excellent adsorption performance of PCFH to RhB can be explained by the pore filling, the π–π interaction,[48] the H-bond interaction,[10] and the electrostatic attraction.[49] The huge specific surface area (2480 $m^2\ g^{-1}$) and highly total pore volume (1.33 $cm^3\ g^{-1}$) of PCFH could provide many pore filling sites for adsorbing representative dye RhB molecule. The results of FT-IR and XPS analyses explained that the surface of PCFH contains a large number of functional groups with oxygen and nitrogen atoms, which can may form hydrogen bonds with RhB molecules. Besides, the π–π interaction between π electrons in the graphite structure of PCFH and the RhB aromatic rings is beneficial to the adsorption. In addition, the electrostatic attraction between PCFH with negative zeta potential and cationic dye RhB could also enhance the adsorption performance. Moreover, in order to verify the applicability of PCFH as an adsorbent, the adsorption capacity of PCFH to RhB was compared with other adsorbents and the results were shown in Table S2.† It can be seen from Table S2† that PCFH has a great potential in industrial dye wastewater treatment due to its excellent adsorption capacity to RhB.

4. Conclusions

This is the first time that porous carbon materials were prepared by activating FH (*Irpex lacteus*) with mixed alkali. This work not only opens up the potential carbon sources for porous carbon materials, but also simply obtains porous carbon materials with large specific surface area and abundant functional groups on the surface. Fast adsorption capacity of PCFH to RhB was achieved 765 mg g^{-1} in the initial 5 min, and the maximum adsorption capacity reached 1912 mg g^{-1} at the pH value of 9. In addition, the removal rate of RhB reached 100%, and could still reach 81% after 3 cycles. We will also conduct further research on PCFH in the fields of oxygen reduction reaction, catalytic hydrogen production, supercapacitor energy storage, and other fields.

Conflicts of interest

There are no conflicts to declare.

Acknowledgements

Thanks for the supported by Technological innovation platform of straw comprehensive utilization in Jilin province (No. (2014) C-1). This research was supported by the Science and Technology Project from Education Department of Jilin Province (No. JJKH20190906KJ). This research was also supported by the Development Project from Science and Technology Department of Jilin Province (No. 20190303057SF).

Notes and references

1 Z. Wang, D. Shen, C. Wu and S. Gu, *Green Chem.*, 2018, **20**, 5031–5057.
2 H. Wang, Y. Zhang, Q. Wang, C. Jia, P. Cai, G. Chen, C. Dong and H. Guan, *RSC Adv.*, 2019, **9**, 9126–9135.
3 B. Ma, Y. Huang, Z. Nie, X. Qiu, D. Su, G. Wang, J. Yuan, X. Xie and Z. Wu, *RSC Adv.*, 2019, **9**, 20424–20431.
4 L. Wang, P. Zhou, Y. Guo, J. Zhang, X. Qiu, Y. Guan, M. Yu, H. Zhu and Q. Zhang, *RSC Adv.*, 2019, **9**, 9718–9728.
5 M. B. Ahmed, M. A. H. Johir, J. L. Zhou, H. H. Ngo, L. D. Nghiem, C. Richardson, M. A. Moni and M. R. Bryant, *J. Clean. Prod.*, 2019, **225**, 405–413.
6 P. Liu, Y. Wang and J. Liu, *J. Energy Chem.*, 2019, **34**, 171–185.
7 D. Yu, Y. Ma, M. Chen and X. Dong, *J. Colloid Interface Sci.*, 2019, **537**, 569–578.
8 M. Song, Y. Zhou, X. Ren, J. Wan, Y. Du, G. Wu and F. Ma, *J. Colloid Interface Sci.*, 2019, **535**, 276–286.
9 J. Wang and C. Chen, *Biotechnol. Adv.*, 2006, **24**, 427–451.
10 J. Wang and C. Chen, *Biotechnol. Adv.*, 2009, **27**, 195–226.
11 C. Zhu, W. L. Yang, H. He, C. Yang, J. Yu, X. Wu, G. Zeng, S. Tarre and M. Green, *Chemosphere*, 2018, **200**, 380–387.
12 Y. Zhong, X. Xia, S. Deng, D. Xie, S. Shen, K. Zhang, W. Guo, X. Wang and J. Tu, *Adv. Mater.*, 2018, **30**, 1805165.
13 X. Kang, H. Zhu, C. Wang, K. Sun and J. Yin, *J. Colloid Interface Sci.*, 2018, **509**, 369–383.
14 Q. Wang, Y. Zhang, H. Jiang and C. Meng, *J. Colloid Interface Sci.*, 2019, **534**, 142–155.
15 C. Wang, Y. Xiong, H. Wang and Q. Sun, *J. Colloid Interface Sci.*, 2018, **528**, 349–359.
16 C. Wang, D. Wu, H. Wang, Z. Gao, F. Xu and K. Jiang, *J. Colloid Interface Sci.*, 2018, **523**, 133–143.
17 S. Chen, S. Tang, Y. Sun, G. Wang, H. Chen, X. Yu, Y. Su and G. Chen, *Materials*, 2018, **11**, 1407.
18 S. Chen, G. Chen, H. Chen, Y. Sun, X. Yu, Y. Su and S. Tang, *Colloids Surf., A*, 2019, **568**, 173–183.
19 J. Lei, Q. Guo, W. Yao, T. Duan, P. Chen and W. Zhu, *J. Mater. Chem. A*, 2018, **6**, 10710–10717.
20 W. Zhu, Y. Li, L. Dai, J. Li, X. Li, W. Li, T. Duan, J. Lei and T. Chen, *Chem. Eng. J.*, 2018, **339**, 214–222.

21 W. Zhu, J. Lei, Y. Li, L. Dai, T. Chen, X. Bai, J. Zhou, L. Wang and T. Duan, *Chem. Eng. J.*, 2019, **355**, 777–783.
22 Y. Lian, X. Bai, X. Li, Z. Gao, Z. Hu and G. Hu, *RSC Adv.*, 2017, **7**, 6842.
23 R. Das, C. D. Vecitis, A. Schulze, B. Cao, A. F. Ismail, X. Lu, J. Chen and S. Ramakrishna, *Chem. Soc. Rev.*, 2017, **46**, 6946–7020.
24 C. H. Nguyen and R. Juang, *J. Taiwan Inst. Chem. Eng.*, 2019, **99**, 166–179.
25 L. Zhang, L. Tu, Y. Liang, Q. Chen, Z. Li, C. Li, Z. Wang and W. Li, *RSC Adv.*, 2018, **8**, 42280.
26 H. Yu, T. Wang, W. Dai, X. Li, X. Hu and N. Ma, *RSC Adv.*, 2015, **5**, 63970.
27 H. He, Z. Xiang, X. Chen, H. Chen, H. Huang, M. Wen and C. Yang, *Int. J. Environ. Sci. Technol.*, 2018, **15**, 1491–1500.
28 V. J. Inglezakis, S. G. Poulopoulos and H. Kazemian, *Microporous Mesoporous Mater.*, 2018, **272**, 166–176.
29 Y. Hao, Z. Wang, Z. Wang and Y. He, *Ecotoxicol. Environ. Saf.*, 2019, **168**, 298–303.
30 J. Li, B. Michalkiewicz, J. Min, C. Ma, X. Chen, J. Gong, E. Mijowska and T. Tang, *Chem. Eng. J.*, 2019, **360**, 250–259.
31 H. Sun, B. Yang and A. Li, *Chem. Eng. J.*, 2019, **372**, 65–73.
32 L. Sun, S. Wan, D. Yuan and Z. Yu, *Sci. Total Environ.*, 2019, **664**, 24–36.
33 L. Zhang, Y. Wang, B. Peng, W. Yu, H. Wang, T. Wang, B. Deng, L. Chai, K. Zhang and J. Wang, *Green Chem.*, 2014, **16**, 3926–3934.
34 G. Fischer, S. Braun, R. Thissen and W. Dott, *J. Microbiol. Methods*, 2006, **64**, 63–77.
35 W. Yang, S. Tian, Q. Tang, L. Chai and H. Wang, *J. Colloid Interface Sci.*, 2017, **496**, 496–504.
36 Y. Li, G. Wang, T. Wei, Z. Fan and P. Yan, *Nano Energy*, 2016, **19**, 165–175.
37 L. Peng, Y. Liang, H. Dong, H. Hu, X. Zhao, Y. Cai, Y. Xiao, Y. Liu and M. Zheng, *J. Power Sources*, 2018, **77**, 151–160.
38 N. Díez, G. A. Ferrero, M. Sevilla and A. B. Fuertes, *J. Mater. Chem. A*, 2019, **7**, 14280–14290.
39 Y. Liu, S. Huang, X. Zhao and Y. Zhang, *Colloids Surf., A*, 2018, **539**, 1–10.
40 T. Wang, P. Zhao, N. Lu, H. Chen, C. Zhang and X. Hou, *Chem. Eng. J.*, 2016, **295**, 403–413.
41 Y. Cheng, C. Yang, H. He, G. Zeng, K. Zhao and Z. Yan, *J. Environ. Eng.*, 2016, **142**, C4015001.
42 M. Wu, H. Liu and C. Yang, *Int. J. Environ. Res. Public Health.*, 2019, **16**, 205.
43 X. Inthapanya, S. Wu, Z. Han, G. Zeng, M. Wu and C. Yang, *Environ. Sci. Pollut. Res.*, 2019, **26**, 5944–5954.
44 Y. Huang, C. Yang, Z. Sun, G. Zeng and H. He, *RSC Adv.*, 2015, **5**, 11475.
45 Y. Guo, J. Zhao, H. Zhang, S. Yang, J. Qi, Z. Wang and H. Xu, *Dyes Pigments*, 2005, **66**, 123–128.
46 J. Zhang, X. Hu, X. Yan, R. Feng, M. Zhou and J. Xue, *Colloids Surf., A*, 2019, **575**, 10–17.
47 H. Zeng, M. Gao, T. Shen and F. Ding, *Colloids Surf., A*, 2018, **555**, 746–753.
48 Y. Gao, Y. Li, L. Zhang, H. Huang, J. Hu, S. Shah and X. Su, *J. Colloid Interface Sci.*, 2012, **368**, 540–546.
49 B. Huang, Y. Liu, B. Li, S. Liu, G. Zeng, Z. Zeng, X. Wang, Q. Ning, B. Zheng and C. Yang, *Carbohydr. Polym.*, 2017, **157**, 576–585.